NeuroImage 78 (2013) 46–58

Contents lists available at SciVerse ScienceDirect

NeuroImage

journal homepage: www.elsevier.com/locate/ynimg

Subregions of the human superior frontal gyrus and their connections

Wei Li [a,1], Wen Qin [a,1], Huaigui Liu [a], Lingzhong Fan [b], Jiaojian Wang [b], Tianzi Jiang [b,*], Chunshui Yu [a,**]

[a] Department of Radiology, Tianjin Medical University General Hospital, Tianjin 300052, PR China
[b] LIAMA Center for Computational Medicine, National Laboratory of Pattern Recognition, Institute of Automation, Chinese Academy of Sciences, Beijing 100190, PR China

ARTICLE INFO

Article history:
Accepted 5 April 2013
Available online 13 April 2013

Keywords:
Diffusion tensor imaging
Superior frontal gyrus
Tractography
Parcellation
Resting-state
Fingerprint

ABSTRACT

The superior frontal gyrus (SFG) is located at the superior part of the prefrontal cortex and is involved in a variety of functions, suggesting the existence of functional subregions. However, parcellation schemes of the human SFG and the connection patterns of each subregion remain unclear. We firstly parcellated the human SFG into the anteromedial (SFGam), dorsolateral (SFGdl), and posterior (SFGp) subregions based on diffusion tensor tractography. The SFGam was anatomically connected with the anterior and mid-cingulate cortices, which are critical nodes of the cognitive control network and the default mode network (DMN). The SFGdl was connected with the middle and inferior frontal gyri, which are involved in the cognitive execution network. The SFGp was connected with the precentral gyrus, caudate, thalamus, and frontal operculum, which are nodes of the motor control network. Resting-state functional connectivity analysis further revealed that the SFGam was mainly correlated with the cognitive control network and the DMN; the SFGdl was correlated with the cognitive execution network and the DMN; and the SFGp was correlated with the sensorimotor-related brain regions. The SFGam and SFGdl were further parcellated into three and two subclusters that are well corresponding to Brodmann areas. These findings suggest that the human SFG consists of multiple dissociable subregions that have distinct connection patterns and that these subregions are involved in different functional networks and serve different functions. These results may improve our understanding on the functional complexity of the SFG and provide us an approach to investigate the SFG at the subregional level.

Introduction

The superior frontal gyrus (SFG) is located at the superior part of the prefrontal cortex and is considered to be composed of several cytoarchitecturally different subregions including the Brodmann areas of 6, 8, 9, and 32 (Brodmann, 1909; Petrides and Pandya, 1999, 2002). As summarized in Fig. S1, the SFG has been reported to be involved in a variety of cognitive and motor control tasks. Specifically, the posterior part of the SFG including the supplementary motor area (SMA) is mainly activated by motor tasks (Chouinard and Paus, 2010; Martino et al., 2011; Nachev et al., 2008); the lateral part of the SFG is involved in execution within working memory (du Boisgueheneuc et al., 2006; Owen, 2000; Owen et al., 1998; Petrides, 2000) and attention (Corbetta et al., 2008; Fox et al., 2006); and the medial part of the SFG is commonly deactivated during the cognitive-related processing and has been ascribed to be a component of the default mode network (DMN) (Buckner et al., 2008; Greicius et al., 2003; Raichle et al., 2001). The above-mentioned evidence suggests the existence of subregions in the human SFG. Furthermore, each SFG subregion is supposed to have its unique connection pattern and to participate in its specific function. However, the SFG has always been described as a single brain area and few studies have focused on the anatomical and functional heterogeneities of the SFG, especially the distinct connection patterns of the SFG subregions.

Most of our knowledge concerning subregions of a structure of interest comes from post-mortem analyses of cyto- or myeloarchitectures (Vogt et al., 1995; Zilles and Amunts, 2009, 2010), which enables us to parcellate the human cortex at a microscopic resolution (Schleicher et al., 1999). However, these methods only consider the internal microstructure of a brain area and not its connections to other brain areas. A connectivity-based parcellation will provide additional information to improve our understanding of the structural and functional specializations of a particular brain area. Diffusion tensor tractography (DTT) can show inter-regional anatomical connectivity in vivo (Johansen-Berg and Rushworth, 2009) and has been extensively used to parcellate heterogeneous brain regions based on their anatomical connection patterns, such as the thalamus (Behrens et al., 2003b), the medial frontal cortex (Johansen-Berg et al., 2004), the cingulate cortex (Beckmann et al., 2009), and the amygdala (Bach et al., 2011). The parcellation

* Correspondence to: T. Jiang, National Laboratory of Pattern Recognition, Institute of Automation, Chinese Academy of Sciences, Beijing 100190, PR China. Fax: +86 10 62551993.
** Correspondence to: C. Yu, Department of Radiology, Tianjin Medical University General Hospital, No. 154, Anshan Road, Heping District, Tianjin 300052, PR China. Fax: +86 22 60362990.
E-mail addresses: jiangtz@nlpr.ia.ac.cn (T. Jiang), chunshuiyu@yahoo.cn (C. Yu).
[1] These authors contributed equally to the work.

1053-8119/$ – see front matter © 2013 Elsevier Inc. All rights reserved.
http://dx.doi.org/10.1016/j.neuroimage.2013.04.011

results were consistent with those from cytoarchitecture and tract tracing studies (Johansen-Berg et al., 2004; Mars et al., 2011).

In contrast with that DTT can exhibit anatomical connection between two brain regions; resting-state functional connectivity (rsFC) can reveal functional correlation between every two regions by evaluating the temporal coherence of the low frequency blood oxygen level dependent (BOLD) signals. The combination of these methods will simultaneously show both the anatomical and functional connection patterns of a brain area, which is essential for understanding its functional specialization. Based on previous cytoarchitectural and functional studies of the SFG in both humans and animals, we hypothesize here that the human SFG includes at least three functionally independent subregions that are involved in different brain functional networks. To test this hypothesis, we applied a DTT-based parcellation scheme to the human SFG using a spectral clustering algorithm and studied the anatomical and functional connection patterns of each SFG subregion from the perspective of functional networks. Then we validated the parcellation result by similar analysis of the bilateral SFGs in another independent data set with different scan parameters. Finally, the anatomical connection pattern of each SFG subregion was investigated by observing fingerprint of each subregion with target regions and the rsFC pattern of each subregion was analyzed by seed-based rsFC analysis.

Materials and methods

Subjects and MRI data acquisition

Two different data sets were obtained in this study. Data set 1 was obtained from 12 healthy, right-handed subjects (5 males; mean age: 25.5 years, range: 22–28 years), whereas data set 2 was obtained from another cohort of 8 healthy, right-handed subjects (3 males; mean age: 22.3 years, range: 19–24 years). Data set 1 included diffusion tensor imaging (DTI), structural MR imaging, and resting-state functional MRI (fMRI) data, whereas data set 2 only included DTI with different scan parameters and structural MR imaging data. All MR images were acquired using a Signa HDx 3.0 T MR scanner (General Electric, Milwaukee, WI, USA) with an eight-channel phased-array head coil. DTI data were acquired by a single-shot echo planar imaging sequence. The DTI parameters of data set 1 were: repetition time (TR) = 15 s; echo time (TE) = 73 ms; matrix = 128 × 128; field of view (FOV) = 256 × 256 mm^2; in-plane resolution = 2 mm × 2 mm; slice thickness = 2 mm without gap; 69 axial slices; 50 non-collinear diffusion gradients (b = 1000 s/mm^2) and 3 non-diffusion-weighted images (b = 0 s/mm^2). Sagittal 3D T1-weighted images were acquired by a brain volume (BRAVO) sequence (TR/TE = 7.8/3.0 ms; FOV = 256 × 256 mm^2; matrix = 256 × 256; in-plane resolution = 1 mm × 1 mm; slice thickness = 1 mm, no gap; 188 slices). The DTI parameters of data set 2 were the same as for data set 1 except for the following: TR = 10 s; TE = 64.2 ms; slice thickness = 3 mm; 45 axial slices; and 55 diffusion gradients. The structural images of data set 2 were the same as for data set 1 except for the following: TR/TE = 8.0/3.0 ms; and 176 slices. The resting-state fMRI data of data set 1 were obtained using a gradient-echo single-shot echo-planar imaging sequence with the following parameters: TR/TE = 2000/30 ms; slice thickness = 3 mm; 1 mm gap; matrix = 64 × 64; FOV = 240 × 240 mm^2; in-plane resolution = 3.75 mm × 3.75 mm; 38 transverse slices; 180 volumes. During fMRI scans, all subjects were instructed to keep their eyes closed, to stay as motionless as possible, to think of nothing in particular, and not to fall asleep. The study was approved by the Medical Research Ethics Committee of Tianjin Medical University, and all participants provided written informed consent forms.

Tractography-based SFG parcellation

ROI definition

The boundaries of the SFG were defined according to descriptions in a prior study (John et al., 2006). The anterior boundary was the anterior termination of the olfactory sulcus, which separated the SFG from the frontal polar; the posterior boundary was the superior part of the precentral sulcus; the infero-lateral boundary was the superior frontal sulcus; and the infero-medial boundary was the cingulate sulcus. According to this definition, the SFG here consisted of BA 6, 8, 9 and 32. The SFG was firstly extracted from the Harvard–Oxford cortical structural atlas with a threshold of 25% minimum probability. Then we manually delineated the region of interest (ROI) of the SFG in the Montreal Neurological Institute (MNI) space according to the boundary definition by John et al. (2006). After that, the seed ROI was transformed back to the individual native DTI space using the inverse of linear transformation and nonlinear deformations. Finally, the seed ROI of the SFG was checked on the coronal, axial and sagittal planes slice-by-slice in every subject to ensure that the ROI of each subject satisfied with the boundary definition by John et al. (2006).

DTI data preprocessing

The DTI and the T1-weighted images were both preprocessed using tools including FMRIB's Diffusion Toolbox (FSL 4.0; http://www.fmrib.ox.ac.uk/fsl) and statistical parametric mapping (SPM8) package (http://www.fil.ion.ucl.ac.uk/spm). After correction for eddy current and head motion, the skull-stripped T1-weighted images were firstly co-registered to the b = 0 images in native DTI space, and then transformed to the MNI space. Finally, the inverted transformation parameters were used to transform the seed and target masks from MNI space to the native DTI space with nearest-neighbor interpolation.

Probabilistic tractography

Probabilistic tractography was performed using the FSL software package. Probability distributions for fiber directions at each voxel were calculated using multiple fiber extension (Behrens et al., 2007) based on a previously published diffusion modeling approach (Behrens et al., 2003a, 2003b). To compensate for the distance-dependent effect, probability counts were corrected by the length of the pathway. Connectivity distribution is the expected length of the pathway that crosses each voxel times the number of samples that cross it (Tomassini et al., 2007). We then estimated the connection probability between each voxel in the seed region and any other voxel of the brain by calculating the number of traces from the seed voxel to the target voxel (any other voxel in the brain). To reduce false positive connections, we thresholded the path distribution estimates using a connection probability of $p < 0.002$ (10 out of 5000 samples). Finally, the connection profiles were stored at a lower resolution of 5 × 5 × 5 mm^3 (Johansen-Berg et al., 2004). Based on the native connectivity matrix, a cross-correlation matrix was calculated that quantified the similarity between the connectivity profiles of the seed voxels (Johansen-Berg et al., 2004).

Tractography-based parcellation

The cross-correlation matrix was then fed into a spectral clustering algorithm with an edge-weighted centroidal Voronoi tessellation for image segmentation (Wang et al., 2009) for automatic clustering. The goal of clustering the cross-correlation matrix was to group together voxels of the seed region that share similar connection profiles with other voxels of the brain. The number of component clusters was, however, chosen by the experimenter.

Selection of cluster number

In order to avoid an arbitrary choice of the number of clusters, we used a cross-validation method to determine the number of clusters which yielded optimal consistency across subjects and hence the optimal number of clusters. Specifically, we employed a leave-one-out

method where each subject's data is left out from the averaging. For each subject, we used Cramer's V to check the consistency between the clustering results of a single subject and the average across the remaining subjects. Cramer's V is a measure of association between two nominal variables and it is calculated based on chi-square (χ^2) statistic (Cramer, 1946, 1999). Here, as an example of 2 clusters, one variable is the category of clusters ($r = 2$) of a single subject and another variable is the category of the average clusters ($c = 2$) across the remaining subjects. According to the frequency distribution of the two variables for each voxel of interest, a 2×2 contingency table was obtained. V is calculated by first calculating chi-square, then using the following calculation:

$$V = \mathrm{SQRT}\left(\chi^2/(n(k-1))\right)$$

where: χ^2 is derived from Pearson's chi-squared test; n is the grand total number of voxels of interest; and k is the number of rows or the number of columns, whichever is less.

Cramer's V gives values within the interval [0, 1] where high values indicate good consistency with a value of 1 indicating a perfect match. The inter-subject consistency was checked for $k = 3, 4, 5, 6, 7$, and 8 clusters.

Maximum probability map (MPM) calculation

Considering inter-individual differences in the SFG parcellation, we calculated the MPM to show the final results (Caspers et al., 2008; Eickhoff et al., 2006). To do this, we transformed each individual parcellation result from diffusion space to the MNI template. The MPM was calculated in the MNI space by assigning each voxel to the subregions to which it was most likely to belong. For each SFG subregion, we also calculated the probabilistic map and distributions of the probability values. The probability map and its corresponding probability distribution reflect the inter-individual variability of each SFG subregion.

Validation

The parcellation results were further validated by the parcellation of the bilateral SFGs in another independent data set (data set 2) using the same parcellation method.

Anatomical connectivity patterns

Anatomical connectivity patterns between each subregion and the whole brain

To elucidate the differential connection patterns of the SFG subregions, the whole brain probabilistic tractography for each subject was run for each subregion in the individual diffusion space by estimating fiber orientations for each seed voxel (Behrens et al., 2007). The fiber connections of each subject were then warped into standard space. The population probability maps of each subregion were derived by overlapping each voxel connected with the seed across subjects and dividing by the number of subjects, so that, a voxel value in the population probability map represents the proportion of the population in whom the voxel is connected with the seed. Here, the threshold for the existence of connection between a seed voxel and a target voxel was defined as $10/5000 = 0.002$.

Target region definition and fingerprints of seed-target area

The target regions were defined by the automated anatomical labeling (AAL) atlas (Tzourio-Mazoyer et al., 2002) that divided each cerebral hemisphere into 45 brain regions. Forty two brain regions on each cerebral hemisphere except for the bilateral medial SFGs, SFGs, and SMAs were defined as target regions. DTT was used to estimate the averaged connection probability between each subregion of the bilateral SFGs and every region of the 42 target regions within the same hemisphere. Finally, we got the top five brain regions that showed the highest connection probability with each SFG subregion. After removing the repetitive regions, we finally obtained 9 target regions in the right SFG and 10 target regions in the left SFG. The only difference between the bilateral SFG target regions was that the putamen was only identified as a target region of the left SFG. To compare the fingerprints of the bilateral SFGs, we computed the fingerprint of each SFG subregion with 9 and 10 target regions, respectively.

Statistical analysis of connection probabilities was performed using SPSS 19.0 (SPSS, Chicago, IL). Repeated-measures analysis of variance (ANOVA) was performed to test the influence of within-subject factors of SFG subregions and target ROIs on the connection probability values.

Resting-state functional connectivity patterns

Resting-state fMRI data preprocessing

The resting-state fMRI data were preprocessed using the Statistical Parametric Mapping (SPM8, http://www.fil.ion.ucl.ac.uk/spm) and Data Processing Assistant for Resting-State fMRI (DPARSF) (Yan and Zang, 2010). The first 10 volumes from each subject were discarded to allow the signal to reach equilibrium and the participants to adapt to the scanning noise. The remaining 170 volumes were corrected for acquisition time delay between different slices. Then, head motion parameters were estimated; none of the subjects had a maximum displacement of >1 mm or a maximum rotation of $>1.0°$. A unified segmentation approach was used to spatially normalize these functional images. The approach included the following steps: (i) individual structural images were coregistered to the mean functional image after motion correction; (ii) the transformed structural images were segmented into gray matter, white matter, and cerebrospinal fluid using a unified segmentation algorithm; and (iii) the motion-corrected functional volumes were spatially normalized to MNI space using the normalized parameters estimated during segmentation, and functional images were then re-sampled into a voxel size of $2 \times 2 \times 2$ mm^3. After normalization, the images were smoothed using a Gaussian kernel of $6 \times 6 \times 6$ mm^3 full-width at half-maximum. Several sources of spurious variances including the estimated motion parameters, linear drift, global average BOLD signals, and average BOLD signals in ventricular and white matter regions were removed from the data through linear regression. Finally, temporal band-pass filtering (0.01–0.08 Hz) was performed on the time series of each voxel to reduce the effects of low-frequency drift and high-frequency noise. Four-dimensional residual time series data in the standard MNI space were acquired for each subject after the preprocessing.

Whole brain rsFC patterns of the SFG subregions

We extracted the ROI of each SFG subregion based on the group clusters using a 90% probability value from anatomical connection probabilistic map, which can reduce crosstalk among the three subregions. For each individual dataset, Pearson correlation coefficients between the mean time series of each seed region and that of each voxel of the whole brain were computed and converted to *z* values using Fisher's *r*-to-*z* transformation to improve the normality. Then, individuals' *z*-values were entered into a random effect one-sample *t* test in a voxel-wise manner to identify brain regions that showed significant positive or negative correlations with the seed region. A paired two-sample *t*-test was used to compare the rsFC strengths between each pair of the SFG subregions. The false discovery rate (FDR) method was used to correct for the multiple comparisons ($p < 0.01$), and only clusters that contained a minimum of 50 voxels were reported here.

Comparison between the anatomical and functional connectivity patterns of the SFG subregions

We calculated the ipsilateral rsFCs between each SFG subregion and the nine target regions derived from anatomical connection

analysis. Statistical analysis of rsFC strength was performed using SPSS 19.0 (SPSS, Chicago, IL). Repeated-measures ANOVA was performed to test the influence of within-subject factors of SFG subregions and target ROIs on the rsFC strength values. To directly compare the anatomical and functional connectivity patterns of each SFG subregion, we rescaled connection strengths into values from 0 to 1. Finally, direct comparisons of anatomical and functional connectivity patterns were realized by fingerprint method.

Further parcellation of SFG subregions

To establish the correspondence between the SFG subregions and the Brodmann areas, the relatively large SFG subregions were further parcellated into subclusters using the same method as the parcellation of the SFG. The connection patterns of these subclusters were also analyzed using the same method as being adopted for the SFG subregions.

Results

Tractography-based parcellation of SFG

In the spectral clustering method, it is important to select an optimal number of clusters. Although there is no gold standard for selecting the cluster number, we selected the optimal cluster number using a cross-validation method based on the consistency of clustering across subjects. We found that a cluster number of 3 gave the highest consistency of clustering across subjects for both the left and right SFGs (Fig. 1).

Using probabilistic tractography and spectral clustering algorithm, the SFG was parcellated into three separable subregions with different anatomical connection patterns. They were the anteromedial SFG (SFGam), the dorsolateral SFG (SFGdl), and the posterior SFG (SFGp) (Fig. 2A). The probabilistic maps of each SFG subregion and the MNI coordinate of the center of gravity for each subregion are shown in Fig. 3. This parcellation scheme was validated by similar analysis of the bilateral SFGs in another independent data set (Fig. 2B). Finally, we found the similar parcellation results and the overlapping rate between the two different data sets was 74.8%, and the matching degree of the bilateral SFGs on data set one was at 73.7%.

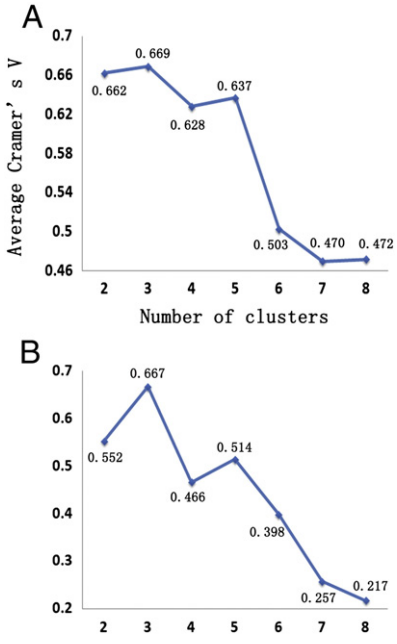

Fig. 1. Average Cramer's V as an indication of clustering consistency in bilateral SFGs (A: left SFG; B: right SFG). The 3-cluster solution has the highest Cramer's V for the superior frontal gyrus.

Anatomical connectivity pattern analysis of SFG subregions

Using probabilistic DTT, we identified the anatomical connection pattern of each SFG subregion (Fig. 4). The SFGam was mainly connected with the anterior cingulate cortex (ACC) and the mid-cingulate cortex (MCC); the SFGdl was connected with the middle and inferior frontal gyri; and the SFGp was connected with the thalamus, precentral gyrus, and inferior frontal gyrus. The average normalized connection strengths between each SFG subregion and the 42 target brain areas of each hemisphere are shown in Fig. 5. After removing the repetitive brain regions, the nine brain regions with higher connection probability to the right SFG subregion were as follows: the ACC, MCC, caudate, posterior cingulate cortex (PCC), middle frontal gyrus, opercular and triangular parts of the inferior frontal gyrus, thalamus, and precentral gyrus. The ten brain regions of the left SFG were the same nine ones as the right SFG except for putamen. For comparison of the bilateral SFGs, nine and ten target regions were selected and the anatomical connectivity fingerprints of seed-target are shown in Figs. 6 and S2.

To quantify the differences in anatomical connections across the three SFG subregions, the connection probabilities with the nine target regions were normalized for the size of individual target ROIs. Normalized connection probabilities were entered in a repeated-measures ANOVA; that test revealed significant differences in the connection patterns across these SFG subregions (Tables 1 and 2). Compared with the SFGdl, the SFGam showed higher probabilities of connection with the ACC, MCC, PCC, and caudate and lower probabilities of connection with the middle frontal gyrus, and the opercular and triangular parts of inferior frontal gyrus. Compared with the SFGp, the SFGam showed higher probabilities of connection with the ACC, MCC, and PCC and lower probabilities of connection with the opercular part of inferior frontal gyrus, precentral gyrus, and thalamus. The SFGdl had higher probabilities of connection with the middle frontal gyrus and the triangular part of inferior frontal gyrus and lower probabilities of connection with the MCC, precentral gyrus, and thalamus than the SFGp.

The rsFC patterns of SFG subregions

The whole brain rsFC map of each SFG subregion is displayed on the Caret PALS template (Van Essen, 2005; Van Essen et al., 2001). Overall, these three SFG subregions showed different rsFC patterns. Because the functional significance of the negative rsFC is a matter of debate, we only focused on the positive rsFCs of each SFG subregion (Fig. 7A, B and Table 3) and just showed the negative rsFCs of the SFG subregions in Fig. 7A, B and Table S1 in the Supplementary materials. Both the SFGam and the SFGdl were correlated with PCC, precuneus, ACC, medial prefrontal cortex, dorsolateral prefrontal cortex, angular gyrus, and anterior temporal lobe. However, the SFGam was also strongly correlated with the MCC, whereas the SFGdl was also strongly correlated with the middle frontal gyrus. The SFGp was correlated with the precentral gyrus, postcentral gyrus, SMA, MCC, and parts of the parietal cortices.

To quantify the differences in rsFCs across the three SFG subregions, the rsFCs were quantitatively compared between every two SFG subregions (Fig. 7C, D). Compared with the SFGdl, the SFGam showed higher rsFC with the MCC and part of prefrontal lobe and showed lower rsFC with the middle frontal gyrus. Compared with the SFGp, the SFGam showed higher rsFC with the MCC and most part of the prefrontal lobe. Compared with the SFGp, the SFGdl showed higher rsFC with the middle frontal gyrus and PCC and showed lower rsFC with the precentral gyrus, postcentral gyrus, and SMA.

Differences in anatomical and functional connectivity patterns of SFG subregions

The rsFCs between each SFG subregion and nine anatomically defined target regions are shown in Table 4. The rsFC strengths were entered into repeated-measures ANOVA; the significant differences in the connection patterns across these SFG subregions are shown in Table 5. The fingerprint method was used to directly compare the anatomical and functional connectivity patterns of each SFG subregion (Fig. 8). Generally, target regions that showed strong anatomical connections with a SFG subregion also had strong rsFCs with that subregion; however, the number of target regions with strong anatomical connections were much less than those that showed strong rsFCs. Specifically, although the SFGam showed strong anatomical and functional connections with the ACC and MCC, it only showed strong rsFCs with PCC, caudate, middle frontal gyrus, thalamus, and the opercular and triangular parts of inferior frontal gyrus. The SFGdl showed higher anatomical and functional connections with middle and inferior frontal gyri; however, it had much weaker rsFCs with the ACC, PCC, and caudate nucleus. The SFGp had strong anatomical and functional connections with the precentral gyrus and opercular part of the inferior frontal gyrus, whereas it only showed strong rsFC with the MCC.

Further parcellation of SFG subregions

The SMA is a part of the SFG and consists of the preSMA and SMA proper. To determine the corresponding relationship between the SMA and the SFG subregions, we parcellated the right SMA into the SMA proper (green color) and preSMA (red color) with a border line of $y = 0$ in the plane of $x = 2$ and $z = 58$ (MNI coordinate) (Fig. S3A). The results are consistent with a pioneer study (Johansen-Berg et al., 2004). As shown in Fig. S3C, the border line between the SFGp (green color) and SFGam (white color) is $y = 4$ in the same x and z planes, suggesting that the SFGp corresponded approximately to the SMA proper (posterior part of BA 6); however, the preSMA is categorized into the SFGam. Then the SFGam was further parcellated using the same method as the parcellation of the SFG. The 2-cluster parcellation resulted in superior and inferior two clusters (Fig. S4A), which are not consistent with the Brodmann areas. We then tested the 3-cluster-scheme and found that the three SFGam subclusters were well corresponding to the Brodmann areas: the anterosuperior subregion of the SFGam (SFGam_as) corresponds approximately to the medial parts of the BA8 and BA9 (green color in Figs. 9A and S4B); the anteroinferior subregion (SFGam_ai) of the SFGam corresponds to the dorsal part of the BA 32 (blue color in Figs. 9A and S4B); and the posterior subregion (SFGam_p) of the SFGam corresponds approximately to the preSMA (anterior portion of the BA 6) (red color in Figs. 9A and S4B). The correspondence between the SFGam_p and the preSMA is shown in Fig. S3B, D. The border line between the SFGam_p (white color in Fig. S3D) and the other two subclusters of the SFGam is $y = 25$ in the planes of $x = 2$ and $z = 58$, which is similar to the anterior border line ($y = 30$) of the preSMA (Fig. S3B). We tried to further parcellate the SFGdl into two subclusters to test if the BA 8 and BA 9 could be separated. The results confirmed our hypothesis that the SFGdl was subdivided into anterior (SFGdl_a) and posterior (SFGdl_p) subregions. The SFGdl_a corresponds to the dorsolateral part of the BA 9 (yellow color in Fig. 9B), and the SFGdl_p corresponds to the dorsolateral part of the BA 8 (orange color in Fig. 9B).

The anatomical connection patterns of the SFGam and SFGdl subclusters

The anatomical connection fingerprints of the SFGam and SFGdl subclusters are shown in Fig. S5. The SFGam_as was anatomically connected with the ACC, MCC, MFG, caudate, and thalamus (Fig. S5A); the SFGam_ai was connected with the ACC and MCC (Fig. S5A); and the SFGam_p was connected with the MCC (Fig. S5A). The SFGdl_a was mainly connected with the MFG, whereas the SFGdl_p was connected with both the MFG and IFG (Fig. S5B).

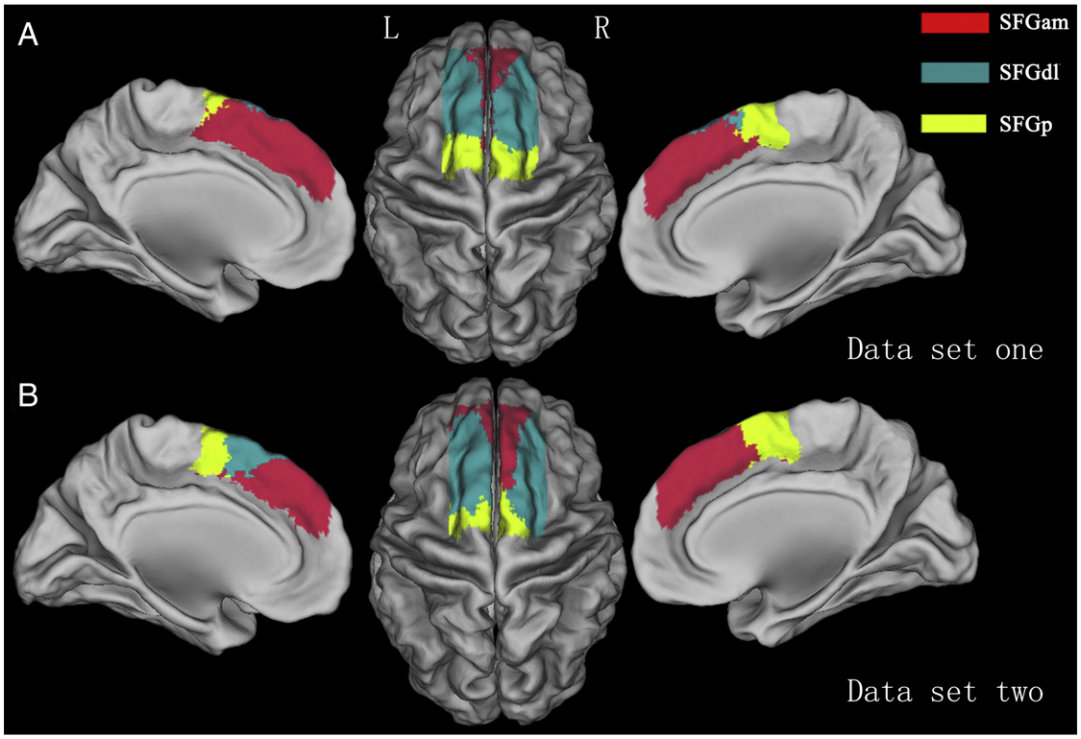

Fig. 2. Connectivity-based parcellation of the human SFG (A) and their validation on another data set (B). The human SFG can be reproducibly subdivided into anteromedial (red), dorsolateral (blue), and posterior (yellow) subregions, as shown in the maximum probabilistic map of the SFG. Abbreviations: L, left; MPM, the maximum probabilistic map; R, right; SFGam, the anteromedial subregion of superior frontal gyrus; SFGdl, the dorsolateral subregion of superior frontal gyrus; SFGp, the posterior subregion of superior frontal gyrus.

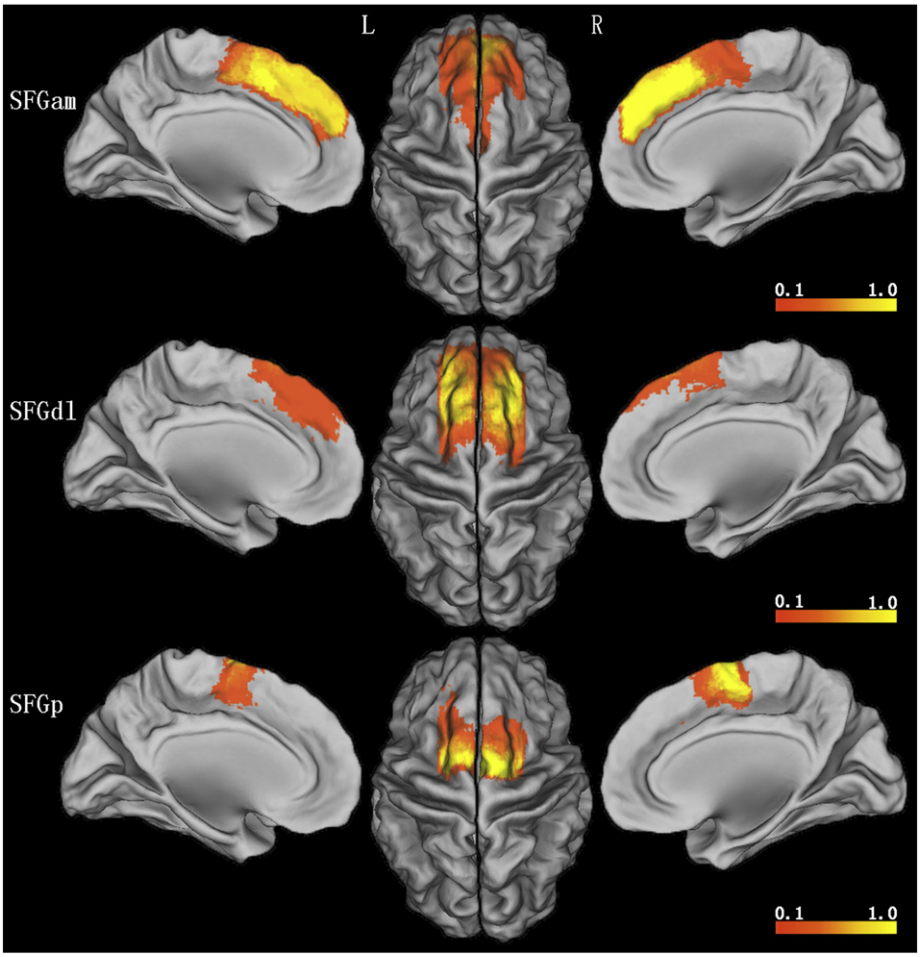

Fig. 3. The probability map of each SFG subregion is displayed on a three dimensional brain surface using the Caret software. Color bar shows the probability of a voxel belonging to a SFG subregion. The coordinates of the center of gravity (MNI) for each cluster: LSFGam (−7, 16, 47), LSFGdl (−19, 23, 50), LSFGp (−19, −4, 62), RSFGam (8, 27, 42), RSFGdl (21, 27, 50), RSFGp (17, −3, 62). Abbreviations: SFGam, the anteromedial subregion of superior frontal gyrus; SFGdl, the dorsolateral subregion of superior frontal gyrus; SFGp, the posterior subregion of superior frontal gyrus.

The functional connectivity patterns of the SFGam and SFGdl subclusters

The functional connectivity patterns of the SFGam subclusters are shown in Tables S2 and S3, and Fig. S6. The SFGam_as was functionally correlated with the anterior MCC, SFG, anterolateral temporal cortex, and inferior parietal lobule (Fig. S6); the SFGam_ai was correlated with the DMN regions (Fig. S6); and the SFGam_p was correlated with the sensorimotor areas, frontoinsular areas, and dorsolateral prefrontal

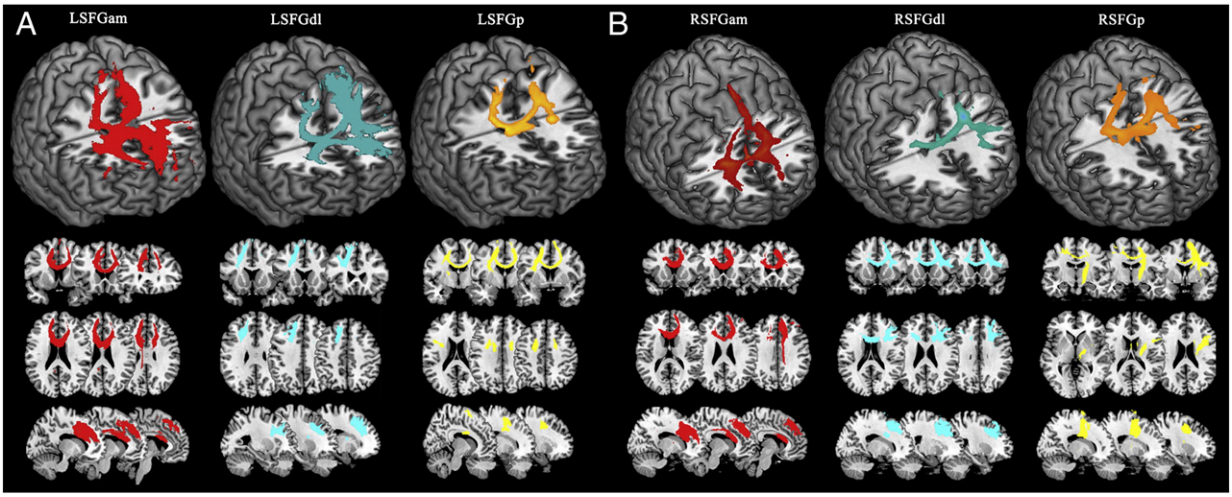

Fig. 4. Whole brain anatomical connection patterns of the left (A) and right (B) SFGam, SFGdl, and SFGp subregions. The fibers of the SFG subregions are shown in different colors (SFGam: red; SFGdl: blue; and SFGp: yellow). Abbreviations: SFGam, the anteromedial subregion of superior frontal gyrus; SFGdl, the dorsolateral subregion of superior frontal gyrus; SFGp, the posterior subregion of superior frontal gyrus.

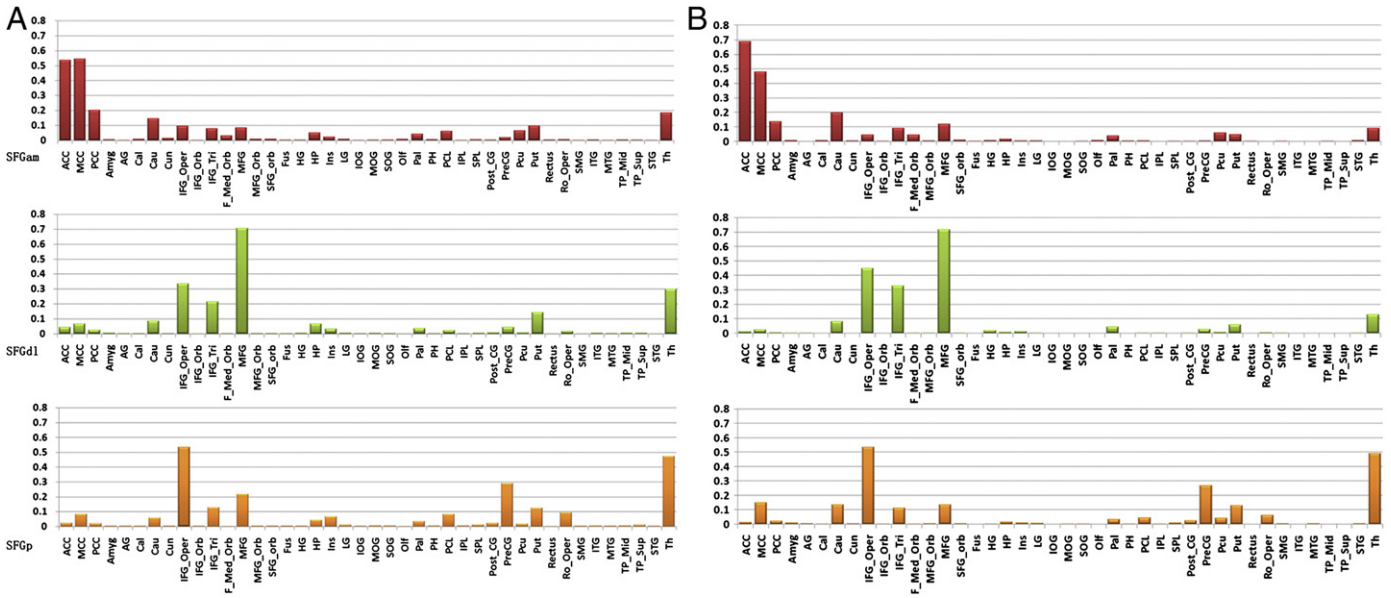

Fig. 5. The average normalized connection strengths between the SFGam, SFGdl, and SFGp subregions and the whole 42 target brain areas (A: left; B: right). Abbreviations: ACC, anterior cingulate cortex; AG, angular gyrus; Amyg, amygdala; Cal, calcarine; Cau, caudate; Cun, cuneus; F_Med_Orb, frontal medial orbital cortex; Fus, fusiform; HG, Heschl gyrus; HP, hippocampus; IFG_Oper, opercular parts of the inferior frontal gyrus; IFG_Orb, orbital part of the inferior frontal gyrus; IFG_Tri, triangular parts of the inferior frontal gyrus; Ins, insula; IOG, inferior occipital gyrus; IPL, parietal_Inferior lobule; ITG, inferior temporal gyrus; LG, lingual gyrus; MCC, mid-cingulate cortex; MFG, middle frontal gyrus; MFG_Orb, orbital part of the middle frontal gyrus; MOG, middle occipital gyrus; MTG, middle temporal gyrus; Olf, olfactory; Pal, pallidum; PCC, posterior cingulate cortex; PCL, paracentral lobule; Pcu, precuneus; PH, paraHippocampal; Post_CG, postcentral gyrus; PreCG, precentral gyrus; Put, putamen; Rectus, rectus; Ro_Oper, rolandic operculum cortex; SFG_Orb, orbital part of the superior frontal gyrus; SMG, supramarginal gyrus; SOG, superior occipital gyrus; SPL, parietal superior lobule; STG, superior temporal gyrus; Th, thalamus; TP_Mid, middle part of the temporal pole; TP_Sup, superior part of the temporal pole.

cortex (DLPFC) (Fig. S6). Quantitative comparisons showed that the SFGam_ai had stronger FC with the ACC of the DMN compared to the SFGam_as; both the SFGam_ai and SFGam_as showed completely different FC patterns when compared with the SFGam_p (Fig. S6). The functional connectivity patterns of the SFGdl subclusters are shown in Tables S4 and S5, and Fig. S7. The SFGdl_a showed a stronger correlation with the DMN, whereas the SFGdl_p demonstrated a stronger correlation with part of the brain that is involved in cognitive control, such as the anterior MCC, DLPFC, and posterior parietal cortex (Fig. S7).

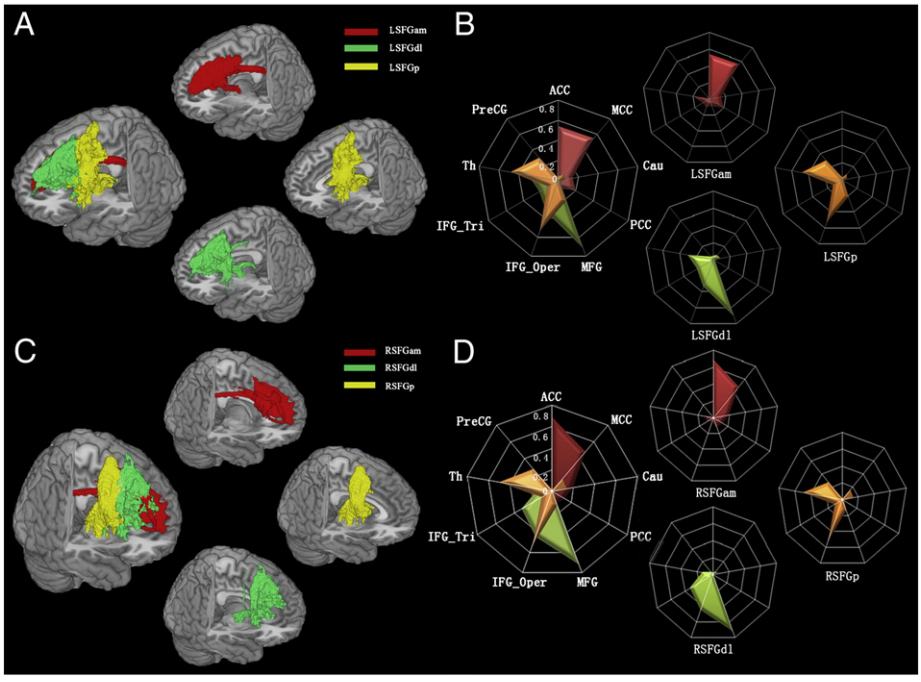

Fig. 6. The anatomical connectivity patterns (A: left; C: right) and fingerprints (B: left; D: right) of the SFG subregions. They are shown in different colors (SFGam: red; SFGdl: green; and SFGp: yellow). Abbreviations: ACC, anterior cingulate cortex; Cau, caudate; IFG_Oper, opercular parts of the inferior frontal gyrus; IFG_Tri, triangular parts of the inferior frontal gyrus; L: left; MCC, mid-cingulate cortex; MFG, middle frontal gyrus; PCC, posterior cingulate cortex; PreCG, precentral gyrus; R: right; SFGam, the anteromedial subregion of superior frontal gyrus; SFGdl, the dorsolateral subregion of superior frontal gyrus; SFGp, the posterior subregion of superior frontal gyrus; Th, thalamus.

Table 1
Averaged anatomical normalized connection strength between SFG subregions and target regions.

	ACC	MCC	PCC	MFG	IFG_Oper	IFG_Tri	PreCG	Cau	Th
LSFGam	**0.536**	**0.543**	0.202	0.085	0.094	0.079	0.019	0.147	0.184
LSFGdl	0.043	0.067	0.026	**0.705**	**0.334**	**0.216**	0.044	0.085	**0.298**
LSFGp	0.024	0.082	0.020	0.217	**0.536**	0.127	**0.290**	0.058	**0.473**
RSFGam	**0.689**	**0.478**	0.136	0.118	0.046	0.091	0.005	0.196	0.091
RSFGdl	0.013	0.025	0.005	**0.715**	**0.448**	**0.327**	0.030	0.082	0.128
RSFGp	0.014	0.151	0.024	0.135	**0.536**	0.113	**0.270**	0.136	**0.492**

The bold emphasizes relatively strong anatomical connection of each SFG subregion. Abbreviations: ACC, anterior cingulate cortex; Cau, caudate; IFG_Oper, opercular parts of the inferior frontal gyrus; IFG_Tri, triangular parts of the inferior frontal gyrus; L, left; SFGam, the anteromedial subregion of superior frontal gyrus; SFGdl, the dorsolateral subregion of superior frontal gyrus; SFGp, the posterior subregion of superior frontal gyrus; MCC, mid-cingulate cortex; MFG, middle frontal gyrus; PCC, posterior cingulate cortex; PreCG, precentral gyrus; R, right; Th, thalamus.

Discussions

To the best of our knowledge, this is the first study to parcellate the human SFG based on anatomical connection patterns and to elucidate the anatomical and functional connectivity patterns of the human SFG at the subregional level. The results of this study show that the human SFG can be subdivided into anteriomedial, dorsolateral, and posterior subregions. The anteriomedial and dorsolateral subregions can be further subdivided into three and two subclusters that are well consistent with the Brodmann areas. Each of these SFG subregions has its specific anatomical and functional connectivity patterns and these subregions are involved in different functional networks. These findings improve our understanding of SFG connectivity and functions at the level of subregions.

Method consideration

In the present study, we parcellated the human SFG based on inter-regional anatomical connection patterns derived from diffusion tensor tractography. The validity and reliability of this method have been extensively confirmed in previous parcellation studies of the human medial frontal cortex (Johansen-Berg et al., 2004), cingulate cortex (Beckmann et al., 2009), thalamus (Behrens et al., 2003b), and amygdala (Bach et al., 2011). In the present study, based on DTI data, we parcellated the SFG into three subregions and further validated the parcellation result in another data set with different scan parameters, suggesting the reproducibility of our method. However, the matching degree between the two different data sets (74.8%) was not as high as we expected, which may be partly explained by individual variation in sulcal patterns (John et al., 2006). Additionally, we just focused on the positive rsFCs because it remains an unsettled debate on the negative rsFCs derived from the resting-state fMRI studies that whether the negative connectivity is an artifact of the global signal regression (Murphy et al., 2009; Weissenbacher et al., 2009) or reflects dynamic, anti-correlated functional networks (Hampson et al., 2010).

SFG subregions

It is well known that the SFG contains four cytoarchitectonic subregions including the BA8, the BA9, the dorsal part of BA 32, and the rostral and dorsal parts of the BA6 (Brodmann, 1909). Each of these BA areas is found to be involved in different functions, such as BA 8 in oculomotor and visuospatial processing (Andersen and Gnadt, 1989; Mountcastle et al., 1975), rostral BA 6 in motor control (Halsband and Passingham, 1982; Petrides, 1982), BA 9 in memory processing (Petrides, 2005), and BA32 in self-relevant processes (Enzi et al., 2009; Kelley et al., 2002). However, this simple partitioned mode is challenged by several lesion studies and functional imaging studies. A lesion study found that only the lateral portions of the SFG (mostly BA 8) contribute to the working memory performance (du Boisgueheneuc et al., 2006). Both task and resting-state fMRI studies have suggested that different parts of the SFG are involved in two anti-correlated networks. One is the task positive network whose brain regions are activated during goal-directed cognitive tasks; the other is the DMN whose brain regions are deactivated during these tasks but they are active during rest. These findings suggest the existence of subregions in the human SFG. Moreover, cytoarchitecture-based parcellation only considers the internal microstructure of a brain area but neglects its connections with other brain areas, which are important for the functional specialization of the brain area.

In the present study, based on the anatomical connection patterns, we parcellated the human SFG into three subregions and validated the parcellation result in another independent imaging data. We further found that each SFG subregion showed its specific anatomical and functional connectivity patterns and is involved in different functional networks. These results not only improve our understanding of the structural and functional specializations of the SFG, but also provide a scheme to investigate the structural and functional characteristics of the SFG at the subregional level.

Connectivity profiles of the SFGam

We found that the SFGam is anatomically connected with the cingulate cortex (mostly the ACC and the MCC) through the cingulum and that it is functionally correlated with the MCC and the DMN. The reciprocally anatomical connections between the SFG and the cingulate cortex have been long appreciated in the macaque (Bates and Goldman-Rakic, 1993; Lu et al., 1994). The dense connections between the DLPFC (including SFG) and the ACC and MCC have also been found in human using DTT (Beckmann et al., 2009). Moreover, the rsFCs between the SFG and the ACC and MCC have been reported (Yu et al., 2011). The anatomical and functional connections between the SFGam and the anterior MCC suggest that the SFGam is involved in cognitive control because the anterior part of the MCC (also named dorsal ACC in many studies) has always been related to cognitive control, such as conflict monitoring (Sohn et al., 2007; Ursu et al., 2009), error detection (Gehring and Fencsik, 2001; Pourtois et al., 2010), response selection (Awh and Gehring, 1999; Paus, 2001), and

Table 2
Differences in the anatomical connections between each pair of the SFG subregions, shown with *p* values (Bonferroni corrected).

SFG subregion	ACC	MCC	PCC	MFG	IFG_Oper	IFG_Tri	PreCG	Cau	Th
LSFGam & LSFGdl	<**0.001**	<**0.001**	0.029	<**0.001**	**0.001**	**0.001**	0.235	0.472	0.382
LSFGam & LSFGp	<**0.001**	<**0.001**	0.030	0.037	<**0.001**	0.257	**0.001**	0.309	0.015
LSFGdl & LSFGp	1.000	0.817	1.000	<**0.001**	0.083	**0.005**	**0.001**	0.794	0.058
RSFGam & RSFGdl	<**0.001**	<**0.001**	**0.001**	<**0.001**	<**0.001**	<**0.001**	1.000	0.040	1.000
RSFGam & RSFGp	<**0.001**	<**0.001**	**0.003**	1.000	<**0.001**	1.000	<**0.001**	0.529	<**0.001**
RSFGdl & RSFGp	1.000	0.030	1.000	<**0.001**	0.785	<**0.001**	<**0.001**	0.670	<**0.001**

The bold emphasizes statistical differences in anatomical connectivity between each pair of the SFG subregions. Abbreviations: ACC, anterior cingulate cortex; Cau, caudate; IFG_Oper, opercular parts of the inferior frontal gyrus; IFG_Tri, triangular parts of the inferior frontal gyrus; L, left; SFGam, the anteromedial subregion of superior frontal gyrus; SFGdl, the dorsolateral subregion of superior frontal gyrus; SFGp, the posterior subregion of superior frontal gyrus; MCC, mid-cingulate cortex; MFG, middle frontal gyrus; PCC, posterior cingulate cortex; PreCG, precentral gyrus; R, right; Th, thalamus.

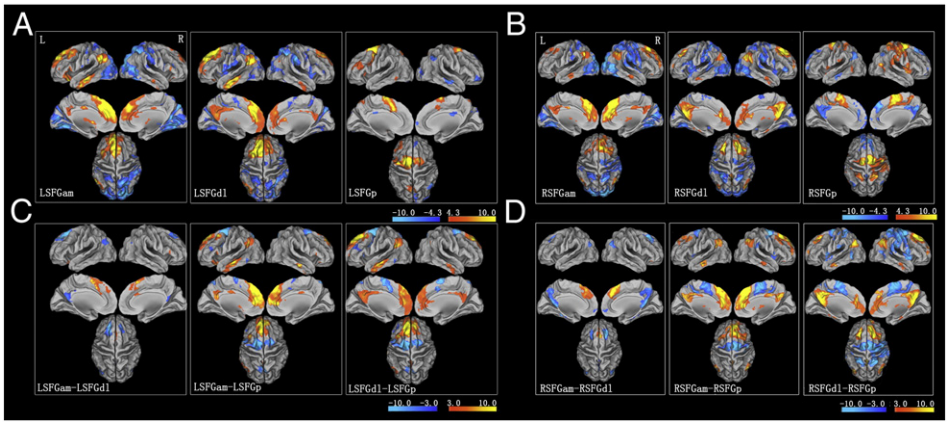

Fig. 7. The rsFC patterns of the left (A) and right (B) SFG subregions and the contrast maps of the rsFCs between every two SFG subregions (C: left; D: right). Abbreviations: L: left; R: right; SFGam, the anteromedial subregion of superior frontal gyrus; SFGdl, the dorsolateral subregion of superior frontal gyrus; SFGp, the posterior subregion of superior frontal gyrus.

attention control (Crottaz-Herbette and Menon, 2006; Luo et al., 2007). Additionally, the SFGam is anatomically connected with the ACC which is a core node of the DMN and functionally correlated with the DMN, which suggests that the SFGam is a node of the DMN and is involved in self-referential processing (Northoff et al., 2006).

Connectivity profiles of the SFGdl

We found that the SFGdl is anatomically connected with the middle frontal gyrus (MFG) and inferior frontal gyrus (IFG) through arcuate fibers, which is consistent with the finding that these lateral prefrontal cortices are reciprocally connected with each other (Kawamura and Naito, 1984; Kinoshita et al., 2012). The lateral prefrontal areas work together to participate in a variety of cognitive functions, such as working memory (Levy and Goldman-Rakic, 2000; Owen, 1997; Owen et al., 1996, 1998), episodic memory (Desgranges et al., 1998; Speck et al., 2000), and attention (Corbetta and Shulman, 2002; Corbetta et al., 2008; Fox et al., 2006). These findings support the SFGdl being engaged in the execution of cognitive manipulations. In addition to the rsFC with the lateral prefrontal areas (mostly MFG), the SFGdl was functionally correlated with the DMN, especially the PCC/precuneus, which is consistent with previous rsFC studies (Ursu et al., 2009; Yu et al., 2011). Although the DMN and the cognitive execution network (CEN) are thought as two functionally anti-correlated networks, they are dynamically interacted and control for the efficient allocation of attention (Leech et al., 2011). The neural substrate for the functional interaction between the two networks has been observed from functional subdivisions of the PCC and the precuneus, in which cognitive subdivisions were identified in both regions (Leech et al., 2011; Margulies et al., 2009). Additionally, the SFG and the PCC are both activated by memory tasks (Carlson et al., 1998; McDermott et al., 1999), which suggests that they are involved in the CEN. Taken all together; we suggest that the dorsolateral part of the SFG may serve as a connection node between the CEN and DMN.

Connectivity profiles of the SFGp

The SFGp corresponds approximately to the SMA proper (Fig. S4A, C) and a part of the premotor cortex and showed anatomical connections with the opercular part of the inferior frontal gyrus, thalamus, precentral gyrus, MCC, and caudate, which is consistent with the anatomical connections of the SMA in monkeys (Jurgens, 1984; Wiesendanger and Wiesendanger, 1985) and those in humans using DTT (Ford et al., 2010; Hyam et al., 2012). All the brain regions are involved in a cortico-striato-thalamo-cortical loop that serves to motor control (such as limb motion and speech) (Seger, 2008; Smits-Bandstra and De Nil, 2007). The rsFC analysis showed that the SFGp is functionally correlated with sensorimotor- and speech-related brain areas, which further supported the function of the SFGp in motor control including speech. In support of this hypothesis, the structural and functional deficits in the SMA were frequently reported in Parkinson's disease (Boylan et al., 2001; Brusa et al., 2006), motor aphasia (Pai, 1999), and stuttering (Chung et al., 2004; Forster and Webster, 2001).

The correspondence between SFG subregions and Brodmann areas

After further parcellation of the SFGam and SFGdl, we established correspondence between the SFG subregions and the Brodmann areas. Specifically, the SFGp corresponds to the posterior BA 6 (SMA proper); the SFGam_p corresponds to the anterior BA 6 (preSMA); the SFGam_as corresponds to the medial parts of the BA8 and BA9; the SFGam_ai corresponds to the dorsal BA 32; the SFGdl_a corresponds to the dorsolateral part of the BA 9; and the SFGdl_p corresponds to the dorsolateral part of the BA 8. These findings are important for understanding the relationship between cytoarchitectural areas and their connection patterns. We also provided an in vivo method to extract each cytoarchitectural area using imaging method.

The subsequent connection analyses of these SFG subclusters further improve our understanding on the specific connection pattern of each Brodmann area within the SFG. Both the SFGp (SMA proper) and SFGam_p (preSMA) are belonged to BA 6 and are connected with sensorimotor areas (Yu et al., 2011); however, the latter shows stronger rsFC with the prefrontal areas (Lu et al., 1994; Luppino et al., 1993; Wang et al., 2005) and brain regions of the salience network (Bonnelle et al., 2012; Duan et al., 2012; Seeley et al., 2007) compared to the former. These findings were also supported by the concept that the medial SFG (preSMA) is involved in the cognitive control network (Sundermann and Pfleiderer, 2012). Although the SFGam_p (BA 6), SFGam_as (BA 8 and 9), and SFGam_ai (BA 32) are initially categorized into a subregion of the SFGam, the latter two subclusters show completely different connection patterns relative to the first one. The SFGam_p (BA 6) is mainly connected with sensorimotor areas, whereas the SFGam_as (BA 8 and 9), and SFGam_ai (BA 32) are mainly connected with cognitive-related regions. However, the connection patterns of the SFGam_as (BA 8 and 9), and SFGam_ai (BA 32) are also slightly different. The former has stronger rsFC with cognitive control areas (Nomura et al., 2010; Vincent et al., 2008), whereas the latter has stronger rsFC with the DMN (Buckner et al., 2008; Greicius et al., 2003; Raichle et al., 2001). Similarly, although the SFGdl_a (BA 9) and SFGdl_p (BA 8) are located in the DLPFC,

Table 3
Brain regions showing positive rsFCs with the SFG subregions.

Seed regions	Connected regions	Peak *t* values	Peak coordinate MNI (x, y, z)	Cluster size (voxels)
LSFGam	B: SFG/SMA/ACC/SFG_Med/Cau/MCC L: MFG/Put/IFG_Orb/Th/IFG_Tri/TP_Sup	26.39	−3, 45, 33	6596
	L: AG/IPL/SMG	14.32	−57, −60, 30	609
	L: ITG/MTG	10.97	−63, −21, −18	569
	R: Cerebelum Crus II/Cerebelum Crus I	9.66	36, −87, −42	373
	L: Pcu/PCC	6.01	−6, −51, 24	155
	R: Cerebelum IX	6.61	6, −51, −45	151
	R: IFG_Orb/IFG_Tri	7.42	57, 27, 9	136
	R: ITG/MTG	8.22	69, −18, −21	133
	R: AG	6.52	63, −57, 33	118
LSFGdl	B: MFG/SFG/SFG_Med/ACC/MCC/PCC/Cau//Pcu L: SMA/IFG_Orb/Rectus/Th	21.43	−15, 36, 48	6683
	L: AG/IPL/MOG	12.53	−45, −63, 27	732
	R: Cerebelum Crus I/Cerebelum Crus II	9.49	42, −81, −39	582
	L: ITG/MTG	12.22	−54, −15, −27	561
	R: ITG/MTG	5.99	51, −12, −39	250
	R: Cerebelum Crus IX	8.30	6, −54, −51	239
	R: AG	8.06	54, −69, 36	231
LSFGp	L: MFG/Put/IFG_Tri/Ins	10.05	−24, 9, −3	702
	L: ITG	5.60	−57, −57, −9	66
RSFGam	B: SFG_Med/ACC R: SFG/MFG/MCC	35.26	6, 39, 30	4792
	R: AG/IPL	10.27	51, −60, 45	786
	L: AG	11.33	−48, −57, 39	655
	B: Pcu	8.17	−3, −15, 33	581
	L: Cerebelum Crus II	6.16	−15, −96, −36	169
	R: Cerebelum IX	7.46	3, −57, −42	142
	L: ITG/MTG	7.86	−66, −15, −24	118
	R: MTG	6.81	66, −15, −18	98
	R: IFG_Orb	8.61	42, 36, −21	89
RSFGdl	B: SFG/MFG/ACC/SFG_Med/F_Med_Orb	22.32	24, 27, 48	3645
	B: Pcu/Cal/MCC/PCC	15.78	15, −54, 24	1889
	R: AG/IPL/MOG	12.69	54, −60, 33	916
	L: AG/MOG	11.37	−42, −81, 42	645
	B: Cerebelum IX	8.72	9, −48, −51	267
	R: ITG/MTG	7.57	66, −12, −21	146
	L: Cerebelum Crus II	6.83	−51, −69, −45	139
	L: MTG	6.56	−63, −18, −27	126
	L: Fus	7.19	−24, −18, −30	104
	R: PH	7.43	27, −21, −24	87
RSFGp	B: Post_CG/PreCG/SMA/MCC R: SFG/SMG/STG/Ro_Oper	26.93	18, −6, 66	6839
	L: SMG/STG	9.11	−54, −33, 21	169
	L: MTG	7.36	−48, −60, 0	107

Abbreviations: ACC, anterior cingulate cortex; AG, angular gyrus; B, bilateral; Cal, calcarine; Cau, caudate; F_Med_Orb, frontal medial orbital cortex; Fus, fusiform; IFG_Orb, inferior frontal gyrus orbital cortex; IFG_Tri, inferior frontal gyrus triangular cortex; Ins, insular; IPL, parietal_Inferior lobule; ITG, inferior temporal gyrus; L, left; MCC, mid-cingulate cortex; MFG, middle frontal gyrus; MNI, Montreal Neurological Institute; MOG, middle occipital gyrus; MTG, middle temporal gyrus; PCC, posterior cingulate cortex; Pcu, precuneus; PH, parahippocampal gyrus; Post_CG, postcentral gyrus; PreCG, precentral gyrus; Put, putamen; R, right; Ro_Oper, rolandic operculum cortex; SFG, superior frontal gyrus; SFGam, the anteromedial subregion of superior frontal gyrus; SFGdl, the dorsolateral subregion of superior frontal gyrus; SFG_Med, superior frontal gyrus medial cortex; SFGp, the posterior subregion of superior frontal gyrus; SMA, supplemental motor area; SMG, supramarginal gyrus; STG, superior temporal gyrus; Th, thalamus; TP_Sup, superior part of temporal pole.

they also have different anatomical and functional connectivity patterns. The SFGdl_a (BA 9) has a stronger correlation with the DMN (Buckner et al., 2008), whereas the SFGdl_p (BA 8) demonstrates a stronger correlation with part of the brain that is involved in cognitive control (Nomura et al., 2010; Vincent et al., 2008).

The differences between the bilateral SFG subregions

We found that the matching degree (73.7%) in the parcellation results between the bilateral SFGs was not as high as we expected, which may be partly caused by inter-hemispheric variations or

Table 4
Functional connectivity strengths between SFG subregions and target regions.

	ACC	MCC	PCC	MFG	IFG_Oper	IFG_Tri	PreCG	Cau	Th
LSFGam	0.544	0.242	0.252	0.500	0.226	0.175	0.024	0.473	0.261
LSFGdl	0.443	0.077	0.521	0.666	**−0.018**	0.009	**−0.144**	0.405	0.234
LSFGp	**−0.069**	0.140	**−0.270**	0.295	0.271	0.254	0.435	0.124	0.193
RSFGam	0.632	0.270	0.291	0.486	0.077	0.149	**−0.368**	0.376	0.277
RSFGdl	0.403	0.267	0.537	0.337	**−0.178**	**−0.221**	**−0.372**	0.251	0.242
RSFGp	**−0.183**	0.103	**−0.285**	**−0.052**	0.253	0.094	0.578	**−0.206**	**−0.066**

The bold emphasizes negative functional connectivity between SFG subregions and target regions. Abbreviations: ACC, anterior cingulate cortex; Cau, caudate; IFG_Oper, opercular parts of the inferior frontal gyrus; IFG_Tri, triangular parts of the inferior frontal gyrus; L, left; SFGam, the anteromedial subregion of superior frontal gyrus; SFGdl, the dorsolateral subregion of superior frontal gyrus; SFGp, the posterior subregion of superior frontal gyrus; MCC, mid-cingulate cortex; MFG, middle frontal gyrus; PCC, posterior cingulate cortex; PreCG, precentral gyrus; R, right; Th, thalamus.

Table 5
Differences in the functional connectivity between each pair of the SFG subregions, shown with *p* values (Bonferroni corrected).

SFG subregion	ACC	MCC	PCC	MFG	IFG_Oper	IFG_Tri	PreCG	Cau	Th
LSFGam & LSFGdl	0.438	0.017	**0.003**	0.032	0.027	0.107	0.013	0.583	1.000
LSFGam & LSFGp	<**0.001**	0.432	<**0.001**	0.078	1.000	0.862	<**0.001**	<**0.001**	1.000
LSFGdl & LSFGp	<**0.001**	1.000	<**0.001**	**0.001**	0.015	0.026	<**0.001**	0.015	1.000
RSFGam & RSFGdl	0.014	1.000	**0.002**	0.172	**0.005**	<**0.001**	1.000	0.094	1.000
RSFGam & RSFGp	<**0.001**	0.588	<**0.001**	<**0.001**	0.351	1.000	<**0.001**	<**0.001**	0.052
RSFGdl & RSFGp	<**0.001**	0.510	<**0.001**	0.006	<**0.001**	0.006	<**0.001**	**0.001**	0.044

The bold emphasizes statistical differences in functional connectivity between each pair of the SFG subregions. Abbreviations: ACC, anterior cingulate cortex; Cau, caudate; IFG_Oper, opercular parts of the inferior frontal gyrus; IFG_Tri, triangular parts of the inferior frontal gyrus; L, left; SFGam, the anteromedial subregion of superior frontal gyrus; SFGdl, the dorsolateral subregion of superior frontal gyrus; SFGp, the posterior subregion of superior frontal gyrus; MCC, mid-cingulate cortex; MFG, middle frontal gyrus; PCC, posterior cingulate cortex; PreCG, precentral gyrus; R, right; Th, thalamus.

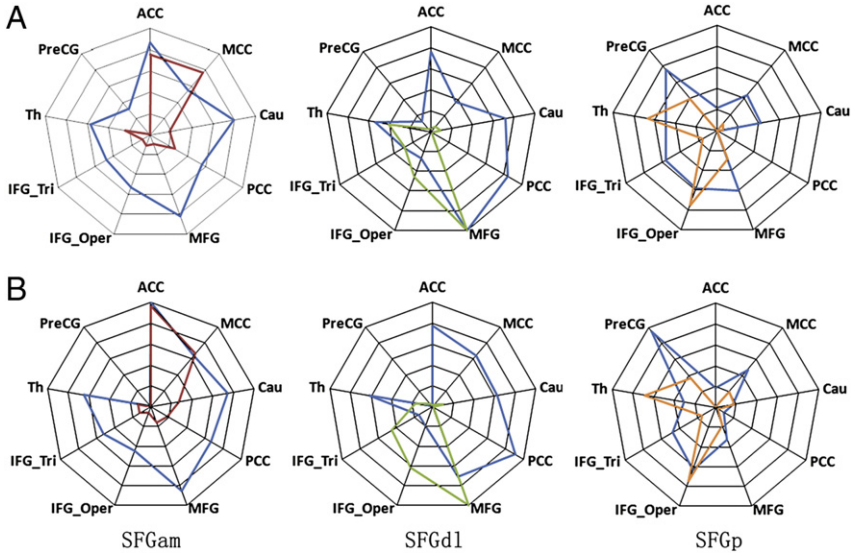

Fig. 8. The comparisons between anatomical and functional connectivity patterns of the SFGam (left column), SFGdl (middle column), and SFGp (right column) of the left (A) and right (B) hemispheres. Red, green and yellow lines represent the anatomical connections of the SFGam, SFGdl, and SFGp, respectively; blue line represents the functional connection of each SFG subregion. Abbreviations: ACC, anterior cingulate cortex; Cau, caudate; IFG_Oper, opercular parts of the inferior frontal gyrus; IFG_Tri, triangular parts of the inferior frontal gyrus; MCC, mid-cingulate cortex; MFG, middle frontal gyrus; PCC, posterior cingulate cortex; PreCG, precentral gyrus; SFGam, the anteromedial subregion of superior frontal gyrus; SFGdl, the dorsolateral subregion of superior frontal gyrus; SFGp, the posterior subregion of superior frontal gyrus; Th, thalamus.

differences in sulcal patterns (John et al., 2006), anatomical connections, and functional lateralization (Fletcher et al., 1997). The anatomical and functional connection patterns of each pair of the SFG subregions (left versus right) were very similar, suggesting no significant lateralization in the connections of the SFG subregions. Of course, there existed subtle differences in anatomical and functional connection strengths between the left and right SFG subregions. These subtle differences cannot simply be ascribed to hemispheric lateralization because several other factors, such as small sample size, individual variation, and difference in seed ROI location, could not be excluded. The lateralization in connections of SFG subregion should be further studied because the functional lateralization of the prefrontal cortex has been reported (Fletcher et al., 1997).

Differences between anatomical and functional connection patterns

We found that brain regions with strong anatomical connection with a SFG subregion also had strong functional connectivity with that subregion, which is consistent with the statement that anatomical connection is the neural basis of functional connectivity (Greicius et al., 2009; Petrides, 2005). However, many brain areas only showed strong functional connectivity with a SFG subregion. That is to say, a SFG subregion had more extensive functional connectivity than anatomical connections. These findings are consistent with previous observations (Eickhoff et al., 2010) and suggest that a very weak anatomical connection between two regions may still hold a high functional significance (Friston, 2002; Grefkes et al., 2008). It is more likely that the functional connectivity may reflect both direct and indirect anatomical connections between two brain regions.

Conclusions

In the present study, we demonstrated that the human SFG can be parcellated into distinct subregions based on their anatomical connection profiles. This parcellation framework can be used to study the structural and functional characteristics at the level of subregion. We also found different anatomical and functional connectivity patterns of these SFG subregions, suggesting that they belong to different functional networks and subserve different functions. These findings may improve our understanding of the SFG from the perspective of connectivity.

Acknowledgments

This study was supported by grants from the National Basic Research Program of China (973 program, 2011CB707801), and the Natural Science Foundation of China (81271551, 30370434, 30730036, and 81201152).

Disclosure: The authors have reported no conflicts of interest.

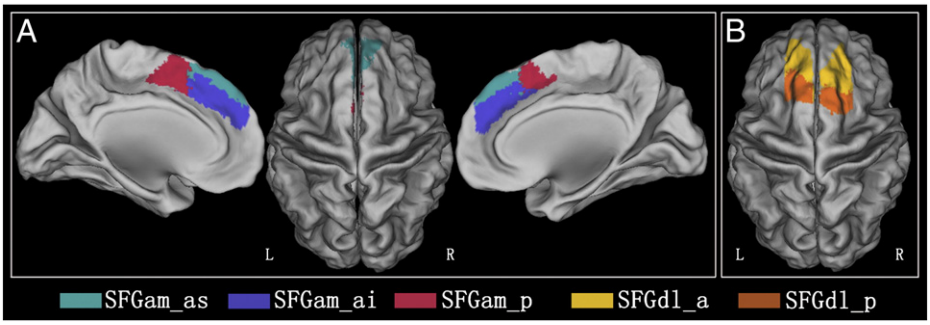

Fig. 9. The MPMs of further parcellation of the SFGam and SFGdl. A: The parcellation of the bilateral SFGam subregions into three subclusters (the anterosuperior part of SFGam: SFGam_as; the anteroinferior part of SFGam: SFGam_ai; the posterior part of SFGam: SFGam_p). B: The parcellation of the bilateral SFGdl subregions into two subclusters (the anterior part of SFGdl: SFGdl_a; the posterior part of SFGdl: SFGdl_p). Abbreviations: L: left; MPM, the maximum probabilistic map; R: right; SFGam, the anteromedial subregion of superior frontal gyrus; SFGdl, the dorsolateral subregion of superior frontal gyrus; SFGp, the posterior subregion of superior frontal gyrus.

Appendix A. Supplementary data

Supplementary data to this article can be found online at http://dx.doi.org/10.1016/j.neuroimage.2013.04.011.

References

Andersen, R.A., Gnadt, J.W., 1989. Posterior parietal cortex. Rev. Oculomot. Res. 3, 315–335.

Awh, E., Gehring, W.J., 1999. The anterior cingulate cortex lends a hand in response selection. Nat. Neurosci. 2, 853–854.

Bach, D.R., Behrens, T.E., Garrido, L., Weiskopf, N., Dolan, R.J., 2011. Deep and superficial amygdala nuclei projections revealed in vivo by probabilistic tractography. J. Neurosci. 31, 618–623.

Bates, J.F., Goldman-Rakic, P.S., 1993. Prefrontal connections of medial motor areas in the rhesus monkey. J. Comp. Neurol. 336, 211–228.

Beckmann, M., Johansen-Berg, H., Rushworth, M.F., 2009. Connectivity-based parcellation of human cingulate cortex and its relation to functional specialization. J. Neurosci. 29, 1175–1190.

Behrens, T.E., Johansen-Berg, H., Woolrich, M.W., Smith, S.M., Wheeler-Kingshott, C.A., Boulby, P.A., Barker, G.J., Sillery, E.L., Sheehan, K., Ciccarelli, O., Thompson, A.J., Brady, J.M., Matthews, P.M., 2003a. Non-invasive mapping of connections between human thalamus and cortex using diffusion imaging. Nat. Neurosci. 6, 750–757.

Behrens, T.E., Woolrich, M.W., Jenkinson, M., Johansen-Berg, H., Nunes, R.G., Clare, S., Matthews, P.M., Brady, J.M., Smith, S.M., 2003b. Characterization and propagation of uncertainty in diffusion-weighted MR imaging. Magn. Reson. Med. 50, 1077–1088.

Behrens, T.E., Berg, H.J., Jbabdi, S., Rushworth, M.F., Woolrich, M.W., 2007. Probabilistic diffusion tractography with multiple fibre orientations: what can we gain? NeuroImage 34, 144–155.

Bonnelle, V., Ham, T.E., Leech, R., Kinnunen, K.M., Mehta, M.A., Greenwood, R.J., Sharp, D.J., 2012. Salience network integrity predicts default mode network function after traumatic brain injury. Proc. Natl. Acad. Sci. U. S. A. 109, 4690–4695.

Boylan, L.S., Pullman, S.L., Lisanby, S.H., Spicknall, K.E., Sackeim, H.A., 2001. Repetitive transcranial magnetic stimulation to SMA worsens complex movements in Parkinson's disease. Clin. Neurophysiol. 112, 259–264.

Brodmann, K., 1909. Vergleichende lokalisationslehre der grobhirnrinde. Barth, Leipzig.

Brusa, L., Versace, V., Koch, G., Iani, C., Stanzione, P., Bernardi, G., Centonze, D., 2006. Low frequency rTMS of the SMA transiently ameliorates peak-dose LID in Parkinson's disease. Clin. Neurophysiol. 117, 1917–1921.

Buckner, R.L., Andrews-Hanna, J.R., Schacter, D.L., 2008. The brain's default network: anatomy, function, and relevance to disease. Ann. N. Y. Acad. Sci. 1124, 1–38.

Carlson, S., Martinkauppi, S., Rama, P., Salli, E., Korvenoja, A., Aronen, H.J., 1998. Distribution of cortical activation during visuospatial n-back tasks as revealed by functional magnetic resonance imaging. Cereb. Cortex 8, 743–752.

Caspers, S., Eickhoff, S.B., Geyer, S., Scheperjans, F., Mohlberg, H., Zilles, K., Amunts, K., 2008. The human inferior parietal lobule in stereotaxic space. Brain Struct. Funct. 212, 481–495.

Chouinard, P.A., Paus, T., 2010. What have we learned from "perturbing" the human cortical motor system with transcranial magnetic stimulation? Front. Hum. Neurosci. 4, 173.

Chung, S.J., Im, J.H., Lee, J.H., Lee, M.C., 2004. Stuttering and gait disturbance after supplementary motor area seizure. Mov. Disord. 19, 1106–1109.

Corbetta, M., Shulman, G.L., 2002. Control of goal-directed and stimulus-driven attention in the brain. Nat. Rev. Neurosci. 3, 201–215.

Corbetta, M., Patel, G., Shulman, G.L., 2008. The reorienting system of the human brain: from environment to theory of mind. Neuron 58, 306–324.

Cramer, H., 1946. Mathematical Methods of Statistics. Princeton University Press, Princeton, NJ.

Cramer, H., 1999. Mathematical Methods of Statistics. Princeton University Press, Princeton, NJ.

Crottaz-Herbette, S., Menon, V., 2006. Where and when the anterior cingulate cortex modulates attentional response: combined fMRI and ERP evidence. J. Cogn. Neurosci. 18, 766–780.

Desgranges, B., Baron, J.C., Eustache, F., 1998. The functional neuroanatomy of episodic memory: the role of the frontal lobes, the hippocampal formation, and other areas. NeuroImage 8, 198–213.

du Boisgueheneuc, F., Levy, R., Volle, E., Seassau, M., Duffau, H., Kinkingnehun, S., Samson, Y., Zhang, S., Dubois, B., 2006. Functions of the left superior frontal gyrus in humans: a lesion study. Brain 129, 3315–3328.

Duan, X., Liao, W., Liang, D., Qiu, L., Gao, Q., Liu, C., Gong, Q., Chen, H., 2012. Large-scale brain networks in board game experts: insights from a domain-related task and task-free resting state. PLoS One 7, e32532.

Eickhoff, S.B., Heim, S., Zilles, K., Amunts, K., 2006. Testing anatomically specified hypotheses in functional imaging using cytoarchitectonic maps. NeuroImage 32, 570–582.

Eickhoff, S.B., Jbabdi, S., Caspers, S., Laird, A.R., Fox, P.T., Zilles, K., Behrens, T.E., 2010. Anatomical and functional connectivity of cytoarchitectonic areas within the human parietal operculum. J. Neurosci. 30, 6409–6421.

Enzi, B., de Greck, M., Prosch, U., Tempelmann, C., Northoff, G., 2009. Is our self nothing but reward? Neuronal overlap and distinction between reward and personal relevance and its relation to human personality. PLoS One 4.

Fletcher, P.C., Frith, C.D., Rugg, M.D., 1997. The functional neuroanatomy of episodic memory. Trends Neurosci. 20, 213–218.

Ford, A., McGregor, K.M., Case, K., Crosson, B., White, K.D., 2010. Structural connectivity of Broca's area and medial frontal cortex. NeuroImage 52, 1230–1237.

Forster, D.C., Webster, W.G., 2001. Speech–motor control and interhemispheric relations in recovered and persistent stuttering. Dev. Neuropsychol. 19, 125–145.

Fox, M.D., Corbetta, M., Snyder, A.Z., Vincent, J.L., Raichle, M.E., 2006. Spontaneous neuronal activity distinguishes human dorsal and ventral attention systems. Proc. Natl. Acad. Sci. U. S. A. 103, 10046–10051.

Friston, K., 2002. Functional integration and inference in the brain. Prog. Neurobiol. 68, 113–143.

Gehring, W.J., Fencsik, D.E., 2001. Functions of the medial frontal cortex in the processing of conflict and errors. J. Neurosci. 21, 9430–9437.

Grefkes, C., Eickhoff, S.B., Nowak, D.A., Dafotakis, M., Fink, G.R., 2008. Dynamic intra- and interhemispheric interactions during unilateral and bilateral hand movements assessed with fMRI and DCM. NeuroImage 41, 1382–1394.

Greicius, M.D., Krasnow, B., Reiss, A.L., Menon, V., 2003. Functional connectivity in the resting brain: a network analysis of the default mode hypothesis. Proc. Natl. Acad. Sci. U. S. A. 100, 253–258.

Greicius, M.D., Supekar, K., Menon, V., Dougherty, R.F., 2009. Resting-state functional connectivity reflects structural connectivity in the default mode network. Cereb. Cortex 19, 72–78.

Halsband, U., Passingham, R., 1982. The role of premotor and parietal cortex in the direction of action. Brain Res. 240, 368–372.

Hampson, M., Driesen, N., Roth, J.K., Gore, J.C., Constable, R.T., 2010. Functional connectivity between task-positive and task-negative brain areas and its relation to working memory performance. Magn. Reson. Imaging 28, 1051–1057.

Hyam, J.A., Owen, S.L., Kringelbach, M.L., Jenkinson, N., Stein, J.F., Green, A.L., Aziz, T.Z., 2012. Contrasting connectivity of the ventralis intermedius and ventralis oralis posterior nuclei of the motor thalamus demonstrated by probabilistic tractography. Neurosurgery 70, 162–169 (discussion 169).

Johansen-Berg, H., Rushworth, M.F., 2009. Using diffusion imaging to study human connectional anatomy. Annu. Rev. Neurosci. 32, 75–94.

Johansen-Berg, H., Behrens, T.E., Robson, M.D., Drobnjak, I., Rushworth, M.F., Brady, J.M., Smith, S.M., Higham, D.J., Matthews, P.M., 2004. Changes in connectivity profiles define functionally distinct regions in human medial frontal cortex. Proc. Natl. Acad. Sci. U. S. A. 101, 13335–13340.

John, J.P., Wang, L., Moffitt, A.J., Singh, H.K., Gado, M.H., Csernansky, J.G., 2006. Inter-rater reliability of manual segmentation of the superior, inferior and middle frontal gyri. Psychiatry Res. 148, 151–163.

Jurgens, U., 1984. The efferent and afferent connections of the supplementary motor area. Brain Res. 300, 63–81.

Kawamura, K., Naito, J., 1984. Corticocortical projections to the prefrontal cortex in the rhesus monkey investigated with horseradish peroxidase techniques. Neurosci. Res. 1, 89–103.
Kelley, W.M., Macrae, C.N., Wyland, C.L., Caglar, S., Inati, S., Heatherton, T.F., 2002. Finding the self? An event-related fMRI study. J. Cogn. Neurosci. 14, 785–794.
Kinoshita, M., Shinohara, H., Hori, O., Ozaki, N., Ueda, F., Nakada, M., Hamada, J., Hayashi, Y., 2012. Association fibers connecting the Broca center and the lateral superior frontal gyrus: a microsurgical and tractographic anatomy. J. Neurosurg. 116, 323–330.
Leech, R., Kamourieh, S., Beckmann, C.F., Sharp, D.J., 2011. Fractionating the default mode network: distinct contributions of the ventral and dorsal posterior cingulate cortex to cognitive control. J. Neurosci. 31, 3217–3224.
Levy, R., Goldman-Rakic, P.S., 2000. Segregation of working memory functions within the dorsolateral prefrontal cortex. Exp. Brain Res. 133, 23–32.
Lu, M.T., Preston, J.B., Strick, P.L., 1994. Interconnections between the prefrontal cortex and the premotor areas in the frontal lobe. J. Comp. Neurol. 341, 375–392.
Luo, Q., Mitchell, D., Jones, M., Mondillo, K., Vythilingam, M., Blair, R.J., 2007. Common regions of dorsal anterior cingulate and prefrontal–parietal cortices provide attentional control of distracters varying in emotionality and visibility. NeuroImage 38, 631–639.
Luppino, G., Matelli, M., Camarda, R., Rizzolatti, G., 1993. Corticocortical connections of area F3 (SMA-proper) and area F6 (pre-SMA) in the macaque monkey. J. Comp. Neurol. 338, 114–140.
Margulies, D.S., Vincent, J.L., Kelly, C., Lohmann, G., Uddin, L.Q., Biswal, B.B., Villringer, A., Castellanos, F.X., Milham, M.P., Petrides, M., 2009. Precuneus shares intrinsic functional architecture in humans and monkeys. Proc. Natl. Acad. Sci. U. S. A. 106, 20069–20074.
Mars, R.B., Jbabdi, S., Sallet, J., O'Reilly, J.X., Croxson, P.L., Olivier, E., Noonan, M.P., Bergmann, C., Mitchell, A.S., Baxter, M.G., Behrens, T.E., Johansen-Berg, H., Tomassini, V., Miller, K.L., Rushworth, M.F., 2011. Diffusion-weighted imaging tractography-based parcellation of the human parietal cortex and comparison with human and macaque resting-state functional connectivity. J. Neurosci. 31, 4087–4100.
Martino, J., Gabarros, A., Deus, J., Juncadella, M., Acebes, J.J., Torres, A., Pujol, J., 2011. Intrasurgical mapping of complex motor function in the superior frontal gyrus. Neuroscience 179, 131–142.
McDermott, K.B., Ojemann, J.G., Petersen, S.E., Ollinger, J.M., Snyder, A.Z., Akbudak, E., Conturo, T.E., Raichle, M.E., 1999. Direct comparison of episodic encoding and retrieval of words: an event-related fMRI study. Memory 7, 661–678.
Mountcastle, V.B., Lynch, J.C., Georgopoulos, A., Sakata, H., Acuna, C., 1975. Posterior parietal association cortex of the monkey: command functions for operations within extrapersonal space. J. Neurophysiol. 38, 871–908.
Murphy, K., Birn, R.M., Handwerker, D.A., Jones, T.B., Bandettini, P.A., 2009. The impact of global signal regression on resting state correlations: are anti-correlated networks introduced? NeuroImage 44, 893–905.
Nachev, P., Kennard, C., Husain, M., 2008. Functional role of the supplementary and pre-supplementary motor areas. Nat. Rev. Neurosci. 9, 856–869.
Nomura, E.M., Gratton, C., Visser, R.M., Kayser, A., Perez, F., D'Esposito, M., 2010. Double dissociation of two cognitive control networks in patients with focal brain lesions. Proc. Natl. Acad. Sci. U. S. A. 107, 12017–12022.
Northoff, G., Heinzel, A., de Greck, M., Bermpohl, F., Dobrowolny, H., Panksepp, J., 2006. Self-referential processing in our brain—a meta-analysis of imaging studies on the self. NeuroImage 31, 440–457.
Owen, A.M., 1997. The functional organization of working memory processes within human lateral frontal cortex: the contribution of functional neuroimaging. Eur. J. Neurosci. 9, 1329–1339.
Owen, A.M., 2000. The role of the lateral frontal cortex in mnemonic processing: the contribution of functional neuroimaging. Exp. Brain Res. 133, 33–43.
Owen, A.M., Evans, A.C., Petrides, M., 1996. Evidence for a two-stage model of spatial working memory processing within the lateral frontal cortex: a positron emission tomography study. Cereb. Cortex 6, 31–38.
Owen, A.M., Stern, C.E., Look, R.B., Tracey, I., Rosen, B.R., Petrides, M., 1998. Functional organization of spatial and nonspatial working memory processing within the human lateral frontal cortex. Proc. Natl. Acad. Sci. U. S. A. 95, 7721–7726.
Pai, M.C., 1999. Supplementary motor area aphasia: a case report. Clin. Neurol. Neurosurg. 101, 29–32.
Paus, T., 2001. Primate anterior cingulate cortex: where motor control, drive and cognition interface. Nat. Rev. Neurosci. 2, 417–424.
Petrides, M., 1982. Motor conditional associative-learning after selective prefrontal lesions in the monkey. Behav. Brain Res. 5, 407–413.
Petrides, M., 2000. The role of the mid-dorsolateral prefrontal cortex in working memory. Exp. Brain Res. 133, 44–54.
Petrides, M., 2005. Lateral prefrontal cortex: architectonic and functional organization. Philos. Trans. R. Soc. Lond. B Biol. Sci. 360, 781–795.
Petrides, M., Pandya, D.N., 1999. Dorsolateral prefrontal cortex: comparative cytoarchitectonic analysis in the human and the macaque brain and corticocortical connection patterns. Eur. J. Neurosci. 11, 1011–1036.
Petrides, M., Pandya, D.N., 2002. Comparative cytoarchitectonic analysis of the human and the macaque ventrolateral prefrontal cortex and corticocortical connection patterns in the monkey. Eur. J. Neurosci. 16, 291–310.
Pourtois, G., Vocat, R., N'Diaye, K., Spinelli, L., Seeck, M., Vuilleumier, P., 2010. Errors recruit both cognitive and emotional monitoring systems: simultaneous intracranial recordings in the dorsal anterior cingulate gyrus and amygdala combined with fMRI. Neuropsychologia 48, 1144–1159.
Raichle, M.E., MacLeod, A.M., Snyder, A.Z., Powers, W.J., Gusnard, D.A., Shulman, G.L., 2001. A default mode of brain function. Proc. Natl. Acad. Sci. U. S. A. 98, 676–682.
Schleicher, A., Amunts, K., Geyer, S., Morosan, P., Zilles, K., 1999. Observer-independent method for microstructural parcellation of cerebral cortex: a quantitative approach to cytoarchitectonics. NeuroImage 9, 165–177.
Seeley, W.W., Menon, V., Schatzberg, A.F., Keller, J., Glover, G.H., Kenna, H., Reiss, A.L., Greicius, M.D., 2007. Dissociable intrinsic connectivity networks for salience processing and executive control. J. Neurosci. 27, 2349–2356.
Seger, C.A., 2008. How do the basal ganglia contribute to categorization? Their roles in generalization, response selection, and learning via feedback. Neurosci. Biobehav. Rev. 32, 265–278.
Smits-Bandstra, S., De Nil, L.F., 2007. Sequence skill learning in persons who stutter: implications for cortico-striato-thalamo-cortical dysfunction. J. Fluency Disord. 32, 251–278.
Sohn, M.H., Albert, M.V., Jung, K., Carter, C.S., Anderson, J.R., 2007. Anticipation of conflict monitoring in the anterior cingulate cortex and the prefrontal cortex. Proc. Natl. Acad. Sci. U. S. A. 104, 10330–10334.
Speck, O., Ernst, T., Braun, J., Koch, C., Miller, E., Chang, L., 2000. Gender differences in the functional organization of the brain for working memory. Neuroreport 11, 2581–2585.
Sundermann, B., Pfleiderer, B., 2012. Functional connectivity profile of the human inferior frontal junction: involvement in a cognitive control network. BMC Neurosci. 13, 119.
Tomassini, V., Jbabdi, S., Klein, J.C., Behrens, T.E., Pozzilli, C., Matthews, P.M., Rushworth, M.F., Johansen-Berg, H., 2007. Diffusion-weighted imaging tractography-based parcellation of the human lateral premotor cortex identifies dorsal and ventral subregions with anatomical and functional specializations. J. Neurosci. 27, 10259–10269.
Tzourio-Mazoyer, N., Landeau, B., Papathanassiou, D., Crivello, F., Etard, O., Delcroix, N., Mazoyer, B., Joliot, M., 2002. Automated anatomical labeling of activations in SPM using a macroscopic anatomical parcellation of the MNI MRI single-subject brain. NeuroImage 15, 273–289.
Ursu, S., Clark, K.A., Aizenstein, H.J., Stenger, V.A., Carter, C.S., 2009. Conflict-related activity in the caudal anterior cingulate cortex in the absence of awareness. Biol. Psychol. 80, 279–286.
Van Essen, D.C., 2005. A Population-Average, Landmark- and Surface-based (PALS) atlas of human cerebral cortex. NeuroImage 28, 635–662.
Van Essen, D.C., Drury, H.A., Dickson, J., Harwell, J., Hanlon, D., Anderson, C.H., 2001. An integrated software suite for surface-based analyses of cerebral cortex. J. Am. Med. Inform. Assoc. 8, 443–459.
Vincent, J.L., Kahn, I., Snyder, A.Z., Raichle, M.E., Buckner, R.L., 2008. Evidence for a frontoparietal control system revealed by intrinsic functional connectivity. J. Neurophysiol. 100, 3328–3342.
Vogt, B.A., Nimchinsky, E.A., Vogt, L.J., Hof, P.R., 1995. Human cingulate cortex: surface features, flat maps, and cytoarchitecture. J. Comp. Neurol. 359, 490–506.
Wang, Y., Isoda, M., Matsuzaka, Y., Shima, K., Tanji, J., 2005. Prefrontal cortical cells projecting to the supplementary eye field and presupplementary motor area in the monkey. Neurosci. Res. 53, 1–7.
Wang, J., Ju, L., Wang, X., 2009. An edge-weighted centroidal Voronoi tessellation model for image segmentation. IEEE Trans. Image Process. 18, 1844–1858.
Weissenbacher, A., Kasess, C., Gerstl, F., Lanzenberger, R., Moser, E., Windischberger, C., 2009. Correlations and anticorrelations in resting-state functional connectivity MRI: a quantitative comparison of preprocessing strategies. NeuroImage 47, 1408–1416.
Wiesendanger, R., Wiesendanger, M., 1985. The thalamic connections with medial area 6 (supplementary motor cortex) in the monkey (*Macaca fascicularis*). Exp. Brain Res. 59, 91–104.
Yan, C.G., Zang, Y.F., 2010. DPARSF: a MATLAB toolbox for "pipeline" data analysis of resting-state fMRI. Front. Syst. Neurosci. 4, 13.
Yu, C., Zhou, Y., Liu, Y., Jiang, T., Dong, H., Zhang, Y., Walter, M., 2011. Functional segregation of the human cingulate cortex is confirmed by functional connectivity based neuroanatomical parcellation. NeuroImage 54, 2571–2581.
Zilles, K., Amunts, K., 2009. Receptor mapping: architecture of the human cerebral cortex. Curr. Opin. Neurol. 22, 331–339.
Zilles, K., Amunts, K., 2010. Centenary of Brodmann's map—conception and fate. Nat. Rev. Neurosci. 11, 139–145.